HHS Public Access

Author manuscript

J Med Chem. Author manuscript; available in PMC 2018 November 29.

Published in final edited form as:

J Med Chem. 2018 May 10; 61(9): 4256–4262. doi:10.1021/acs.jmedchem.8b00240.

^{18}F-Positron Emitting/Trimethine Cyanine-Fluorescent Contrast for Image-Guided Prostate Cancer Management

Harikrishna Kommidi[†,▽], **Hua Guo**[†,▽], **Fuad Nurili**[‡], **Yogindra Vedvyas**[†], **Moonsoo M. Jin**[†], **Timothy D. McClure**[§], **Behfar Ehdaie**[⊥], **Haluk B. Sayman**[#], **Oguz Akin**[‡], **Omer Aras**[*,‡], and **Richard Ting**[*,†]

[†]Department of Radiology, Molecular Imaging Innovations Institute, Weill Cornell Medicine, New York, New York 10065, United States

[‡]Department of Radiology, Memorial Sloan Kettering Cancer Center, New York, New York 10065, United States

[§]Department of Urology, Weill Cornell Medicine, New York, New York 10065, United States

[⊥]Urology Service, Department of Surgery, Memorial Sloan Kettering Cancer Center, New York, New York 10065, United States

[#]Department of Nuclear Medicine, Cerrahpasa Medical Faculty, Istanbul University, Fatih, Istanbul 34303, Turkey

Abstract

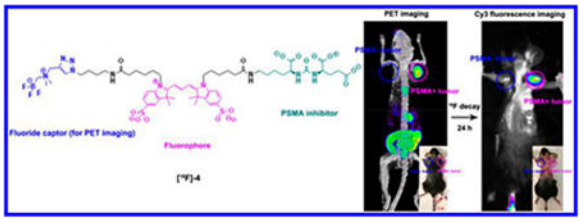

[$^{18/19}$F]-**4**, an anionic GCPII/PSMA inhibitor for image-guided intervention in prostate cancer, is described. [^{19}F]-**4** is radiolabeled with a radiochemical yield that is ≥27% and a molar activity of 190 ± 50 mCi/μmol in a <1 h, one-step, aqueous isotopic exchange reaction. [^{19}F]-**4** allows PSMA expression to be imaged by fluorescence (FL) and [^{18}F]-PET. PC3-PIP (PSMA-positive, EC_{50} = 6.74 ± 1.33 nM) cancers are specifically delineated in mice that bear 3 million (18 mg) PC3-PIP and PC3 (control, PSMA-negative) cells. Colocalization of [$^{18/19}$F]-**4** PET, fluorescence, scintillated biodistribution, and PSMA expression are observed.

[*]**Corresponding Authors**: O.A. (nuclear medicine, radiology): araso@mskcc.org.; R.T. (chemistry, pharmacology): rct2001@med.cornell.edu; phone, (+1) 646-962-6195.

[▽]Author Contributions

H.K and H.G. contributed equally. H.K. designed syntheses and performed radiolabeling. H.G. performed in vivo and in vitro experiments involving animal and cell lines. O.Ak., B.E., O.Ar., and H.S. are responsible for patient related studies.

Supporting Information

The Supporting Information is available free of charge on the ACS Publications website at DOI: 10.1021/acs.jmedchem.8b00240.

Methods for [^{18}F]-**4** preparation, characterization, radiolabeling, and biological evaluation (PDF)

Molecular formula strings (CSV)

The authors declare no competing financial interest.

INTRODUCTION

Prostate cancer (PCa) is a leading cause of mortality among all cancers for men. PCa affects 1 in 6 men and 80% of males over 80 years of age.[1] Radical prostatectomy is a common treatment for localized prostate cancer. In 2009, 192 000 new cases of prostate cancer were reported,[2] and in 2010, 138 000 prostatectomies were performed.[3] This year, 29 430 men in the United States will die due to metastatic disease of prostate origin. Half of these deaths will be in patients who have already undergone treatment with surgery, due to incomplete surgical removal of tumor (including positive tumor margins) leading to distant disease or unrecognized metastases at presentation.[4] These patients may benefit from technology that improves the accuracy of prostatectomy.

Traditional strategies for prostate cancer diagnosis, staging, and detection of PCa metastasis include computed tomography (CT), magnetic resonance imaging (MRI), bone scintigraphy, and [^{18}F]-FDG positron emission tomography (PET). On occasion, these technologies lead to inappropriate surgeries in low-risk patients, unwanted biopsies, and unnecessary prostatectomies.[5,6] Recently, radiolabeled prostate-specific membrane antigen (PSMA) biomarker-specific imaging agents have allowed PCa to be visualized more accurately by SPECT and PET.[7–11] These competitive agents are highly specific to PCa and are useful in presurgical planning and postsurgical evaluation. Unfortunately, SPECT and PET agents are less useful during surgery, as PET and γ-scintillation lacks the resolution (<1 mm) to visualize fine tumor margins or micrometastases within a surgical site.[12]

Intraoperative decision making and choice of surgical technique are critical to a PCa prognosis. Dilemmas are often present during surgery, where a urologist must decide between nerve-sparing and margin resection. Additionally, the extent of lymph node dissection is critical to disease outcomes, where overly aggressive dissections lead to comorbidity. PSMA-targeted fluorophores have been proposed to improve intraoperative decision-making by using intraoperative fluorescence (FL) guidance and tumor margin delineation at high resolution.[13–15]

Recently, these fluorescent technologies have been improved in competitive PSMA-specific strategies that allow visualization by fluorescence and, additionally, by ^{111}In-SPECT or ^{18}F, ^{68}Ga-PET.[16,17] We report the synthesis of [^{18}F]-**4**, a PSMA specific fluorophore that is visible by ^{18}F-PET.

By placing PET and FL modalities on the same molecular ligand, notorious complications associated with co-injected mixtures of separate, stand-alone PET, SPECT, or FL agents can be avoided. These complications include receptor saturation due to limited receptor expression, pharmacological differences in blood clearance, differences in nonspecific tissue accumulation, albumin binding, or PSMA affinity. Regulatory approval (safety) of a PET/FL probe would simultaneously clear two imaging modalities for in vivo use.

RESULTS

[^{19}F]-**4** synthesis is achieved in four steps from Cy3.18.OH (Scheme 1). [^{19}F]-**4** is stable if stored dry at room temperature in solid form. Chemical decomposition (defluoridation) is not observed under physiological conditions. Analogs of [^{19}F]-**4** are not as stable. Initial attempts at excluding the triazole from [^{19}F]-**4** failed (see Supporting Information). Isotope exchange-based radiochemistry first described by Schirrmacher et al.[18] has been adapted by Liu and Perrin et al. to the alkylammoniomethyl trifluoroborate ($AMBF_3$).[19] This $AMBF_3$ moiety is critical in ensuring stable, rapid, and aqueous isotopic exchange ^{18}F-PET chemistry on [^{18}F]-**4**.[19] [^{18}F]-**4** radiolabeling proceeds rapidly (15–20 min) under acidic (pH 2.5) conditions, especially at higher temperatures 80–90 °C. The rate-limiting step in [^{18}F]-**4** production is the separation of [^{18}F]-**4** from [^{18}F]-fluoride ion. This can be performed using C18 Sep-Pak cartridges. This separation must be performed with retarded mobile-phase flow rates. We prefer mechanized purification using a syringe pump (e.g., HST NORM-JECT syringe pump) set to deliver at <40 mL/h. This chromatography can take upward of 40 min and represents the rate limiting step in [^{18}F]-**4** preparation. Future, superior purification matrices[19–21] or precipitative isolation methods could reduce chromatography times. [^{18}F]-**4** is isolated at high radiochemical purity, as observed on reverse phase high-performance liquid chromatography (HPLC) (Figure 1C).

In Vitro Fluorescent Confirmation of Nanomolar [^{18}F]-4-PSMA Specificity.

PSMA expression of PC3-PIP cell lines is confirmed by J591 primary and allophycocyanin (APC) secondary antibody staining (Figure 2A). Very low PSMA expression on commercial PC3 cell lines is observed. Authenticated cell lines are used to demonstrate [^{19}F]-**4** affinity in PSMA expressing cancer. In vitro, [^{19}F]-**4** affinity to PSMA expressing cells is confirmed in duplicate in flow cytometry and epifluorescent microscopy experiments (Figure 2). Epifluorescent microscopy is used to confirm [^{19}F]-**4** membrane localization, indicating labeling of extracellular PSMA expressed on PC3-PIP cell lines (Figure 2C). Fluorescent microscopy indicates [^{19}F]-**4** internalization by PC3-PIP cells, suggesting that [^{19}F]-**4** undergoes endocytosis that is mediated by PSMA binding.

PC3-PIP, PSMA+ cells are used to calculate [^{19}F]-**4** PSMA specific affinity (EC_{50}). PC3, PSMA− cells are used as control for nonspecific [^{19}F]-**4** affinity. Cy3 channel fluorescent flow cytometry demonstrates [^{19}F]-**4**-PC3-PIP EC_{50} at 6.74 ± 1.33 nM (Figure 3B, fluorescence-activated cell sorting (FACS)). Nonspecific binding between [^{19}F]-**4** and PC3 is not observed (Figure 3A).

PET/CT Analysis.

In vivo, [^{19}F]-**4**-PSMA specific binding is assessed in immunocompetent male C57BL/6 mice in PET/CT experiments (Figure 4A). A 3 million count quantity of PC3 and PC3-PIP cells is aliquoted, washed, isolated by centrifugation, and weighed in a tared Eppendorf tube. A 3 million count quantity of PC3 and PC3-PIP cells weighs 18 mg. Cohorts of mice ($n = 6$) receive subcutaneous injections of (a) no cells (1× PBs), (b) 3 million PC3 cells (PSMA−, left flank, 18 mg), or (c) 3 million PC3-PIP cells (PSMA+, right flank, 18 mg). [^{18}F]-**4** (2.5 nmols, 80 μCi) is injected into the tail vein of mice 15 min later. An ^{18}F-PET scan is

performed at 2 and 6 h after injection. [^{18}F]-**4** uptake in PSMA-expressing PC3-PIP containing tissue is clearly visible by PET (Figure 4A bottom, right flank, purple arrow). [^{18}F]-**4** uptake in flank of control (no cell injections) and PC3 containing mouse volumes (PSMA−) are not observed by PET/CT at 2 or 6 h.

Ex Vivo γ-Scintillation.

Biodistribution of [^{18}F]-**4**, 2 h after injection on excised tissue is quantfied using γ-scintillation counter. Tissue and organs harvested from C57BL/6 immunocompetent mice bearing PC3 (PSMA−, left flank) and PC3-PIP (PSMA+, right flank) cells are weighed and quantitated by γ-scintillation (Figure 4B). [^{18}F]-**4** is much greater in right-flank myocutaneous tissue containing PSMA+, PC3-PIP. At least 175-fold less activity is visible in left-flank myocutaneous tissue containing PC3 cells. %ID per gram is calculated by dividing scintillated activity with weights of centrifuged aliquots of 3 million PC3 and PC3-PIP cells are acquired prior to flank injection. Intestinal and kidney signals are significant, indicating that [^{18}F]-**4** is excreted renally and through hepatobiliary routes. Recent studies report that kidneys, proximal small intestine, or salivary glands also express PSMA,[22] which explains PET signal in these tissues. Uptake of [^{18}F]-**4** is not detected in the brain, although NAALADase I is expressed in the brain,[23] suggesting that [^{18}F]-**4** cannot cross the blood–brain barrier in significant quantities. [^{18}F]-**4** is minimally present in the liver, heart, lungs, skin, and blood.

Fluorescence Quantitation.

In vivo/ex vivo fluorescence imaging performed 24 h after injection is used to corroborate [^{18}F]-**4**-PSMA in vivo (Figure 5). All fluorescent data corroborate PET imaging data in Figure 4. [^{18}F]-**4**-Cy3 fluorescence could not be observed through the black fur of C57BL/6 mice. Therefore, hair is removed to observe [^{18}F]-**4** Cy3 fluorescence (Figure 5, left panel, fluorescence intensity is greater after skin removal, center panel). [^{18}F]-**4** fluorescence persists in tissue bearing PC3-PIP, (PSMA+) cells (Figure 5, yellow arrow). A nonquantitative (autofluorescence is significant) fluorescent biodistribution assay is performed on excised tissue (Supporting Information Figure S2). [^{18}F]-**4** fluorescent signal at PC3-PIP cancer is 5.2-fold higher than in PC3 cancer. During prostatectomy, fluorescence data would aid a surgeon in tumor margin confirmation to verify complete tumor resection. [^{19}F]-**4** fluorescence can be used to resolve PSMA+ tumor margins after ^{18}F-PET imaging.

DISCUSSION

We report the synthesis of [$^{18/19}$F]-**4** and demonstrate that [$^{18/19}$F]-**4** is highly specific to PSMA expressing tissue, with an EC_{50} of 6.74 ± 1.33 nM in vitro and a 175-fold (2 h after injection) enhancement in signal in PSMA positive vs PSMA negative prostate cancers by in vivo PET and ex vivo fluorescent imaging, respectively. Little affinity is observed toward non-PSMA expressing tissue. [$^{18/19}$F]-**4** is radiolabeled using aqueous isotopic exchange.[18,24] The electronic structures, and therefore EC_{50} values, of [^{18}F]-**4** and nonradiolabeled [^{19}F]-**4** are identical. [$^{18/19}$F]-**4** is useful in vivo, in PET imaging. Simultaneously, [$^{18/19}$F]-**4**'s fluorescence properties remain useful to surgeons in an intraoperative setting, even 24 h after injection, following quantitative fluoride-18 isotope decay.

Translational Potential.

Biomarker-specific agents like [^{18}F]-**4** would improve the efficacy of prostatectomy by providing persisting, cancer-specific contrast that is useful to the multiple specialists (radiologists, surgeons, and pathologists) who staff our multispecialty teams that currently manage prostate cancer. A single injection of a PET/FL probe allows for (i) presurgical planning, in which PSMA+ primary cancer and lymph node metastases are resolved in PET/MR and PET/CT; (ii) intraoperative, fluorescent-guided resection of a primary tumor and lymph nodes (0.5–72 h after injection); and (iii) margin confirmation in triplicate, i.e., by the surgeon in vivo, with fluorescence, postsurgery, within an open surgical site; by the surgeon ex vivo, by fluorescence in excised tissue; and by the pathologist in fluorescent or nonfluorescent histopathology.[25] [^{19}F]-**4** will be important in intraoperative, frozen section margin determination. Frozen sections are less accurate than permanent, formalin-fixed histopathologic analysis. However, frozen sections can be performed intraoperatively and allow immediate same-surgery revision that can be guided by [^{19}F]-**4**.

Utility in Prostate Cancer.

Overexpression of PSMA in prostate cancer correlates with poorly differentiated, metastatic, and hormone-refractory carcinomas.[26] PSMA is therefore an attractive target for diagnostic and therapeutic approaches to PCa.[27] PSMA is expressed primarily in normal human prostate epithelium and is upregulated in metastatic prostate cancer. Other tissues exhibit low basal amounts of PSMA including kidneys, the proximal small intestine, and salivary glands.[22,28]

Comparable Technologies.

A wide variety of optical and radiopharmaceutical, PSMA-based imaging agents are being investigated. Chen et al. report an ICG-conjugated agent for PSMA-based fluorescence imaging and demonstrate a PSMA inhibitory activity of 0.37 nM, 10-fold higher in PSMA-expressing cancer vs PSMA-deficient cancer.[29] Radiopharmaceutical agents include ^{68}Ga,[30] ^{99m}Tc,[31] ^{125}I,[7] and ^{18}F[32] derivatives that demonstrate renal clearance and nanomolar to subnanomolar affinity to PSMA+ tissue in animal models. While not fluorescent, these compositions have resulted in ongoing clinical trials.[33] Given the current infrastructure dedicated to clinically imaging [^{18}F]-2-fluorodeoxyglucose, we believe that a ^{18}F-construct for imaging PSMA primary and metastatic cancer may be advantageous.

CONCLUSIONS

We describe the synthesis of a PET/FL probe, [^{18}F]-**4**, that is highly specific to PSMA expressing prostate cancer. [^{18}F]-**4** can be visualized by PET/MR, PET/CT, and delayed FL spectroscopy. [^{18}F]-**4** has promise in the noninvasive imaging of PSMA expressing cancers in the prostate and lymph nodes, while FL allows for utility during surgery and in histology, even following comprehensive radioisotope decay. [^{18}F]-**4** will allow PSMA expression to be observed in five ways that are clinically relevant: in vivo, in noninvasive, deep-tissue [^{18}F]-PET imaging; in vivo, in intraoperative fluorescence laparoscopy; ex vivo in γ-scintigraphy; ex vivo, in gross anatomical fluorescent margin delineation; and ex vivo, in fluorescent histology. During surgery, this technology has the potential to improve our

ability to better preserve nerve tissue, completely resect cancer, and detect lymph node micrometastases to extend lymphadenectomy or spare men from lymph node dissection, assuming the negative prediction value of [^{18}F]-**4** is high.

EXPERIMENTAL SECTION

General Synthetic Methods.

Chemicals were purchased from ACROS, Aldrich, Combi-blocks, TCI, or Alfa Aesar. ACUPA was purchased from Astatech (catalog no. W11493). Sterile, endotoxin and mycoplasma free, isotonic 1× PBS (pH 7.4 ± 0.1) was purchased from Corning Cellgro, 21-040-CM. Analytical, reverse phase UPLC–MS was performed on a Waters Acquity H class HPLC/SQD2 mass spectrometer and a Phenomenex Kinetex 1.7 μm C18 100 Å, 50 cm × 2.1 mm i.d. column (00B-4475-AN), with a 1.5 min 10–90% H_2O/acetonitrile (ACN) (0.05% TFA) gradient and a flow rate of 0.6 mL/min (unless stated otherwise). Preparative HPLC was performed on a Agilent 1200 series HPLC equipped on a Phenomenex Luna C18(2) 100 Å, 250 cm × 21.20 mm i.d. 10 μm reverse phase column (00G-4253-P0 AX), with a 40 min 10–90% H_2O/ACN (0.05% TFA) gradient and a flow rate of 12 mL/min. All of the tested compounds had ≥95% purity as evidenced by HPLC, ^{1}H, ^{13}C, and ^{19}F NMR peak integration. Purity of radiolabeling (≥95%) was verified on a Varian reverse phase HPLC, using a Waters SunfireTM C18 3.5 μm, 4.6 mm × 50 mm column (186002551), an attached radiodetector, and a 10–90% H_2O/ACN (0.05% TFA) elution gradient with a flow rate of 2 mL/min. ^{1}H, ^{13}C, and ^{19}F NMR was performed on a 500 MHz Bruker spectrometer. Thermo Scientific 5 mL React-Vial no. 13223 was used for fluoride concentration.

Synthesis.

Reagents and conditions used to synthesize [^{18}F]-**4** are described in Scheme 1. CY3.18.OH is synthesized as described in Mujumdar et al.[34] *N*-Propargyl-*N,N*-dimethylammonium trifluoroborate ($AMBF_3$) is prepared as described by Liu et al.[19] One of two pendant amines on Cy3.18.OH is reacted with an equivalent of *tert*-butyl protected 2-(3-((*S*)-5-amino-1-carboxypentyl)ureido)pentanedioic acid (ACUPA) in the presence of 1-ethyl-3-(3-dimethylaminopropyl)carbodiimide hydrochloride (EDCI) and HOBt for 6 h at room temperature to generate a Cy3-ACUPA intermediate. In situ addition of 1 mol of 1-azidobutylamine and additional EDCI gives the azide bearing precursor **2**, which is isolated by preparative HPLC. *tert*-Butyl ester deprotection of **2** with neat trifluoroacetic acid followed by acid removal in vacuo and same-pot, copper(I) catalyzed 1,3 cycloaddition reaction of azide **2** with $AMBF_3$ 3 gives the target compound [^{19}F]-**4**. [^{19}F]-**4** is stable at physiological pH. Less than 1% [^{19}F]-**4** defluoridation is observed following 7 days of room temperature incubation with fetal bovine serum in ^{19}F NMR fluoride studies (Supporting Information Figure S1).[35]

1-(6-((4-Azidobutyl)amino)-6-oxohexyl)-2-((*E*)-3-((*Z*)-1-((7*R*,11*S*)-7,11-bis(*tert*-butoxycarbonyl)-2,2-dimethyl-4,9,17-trioxo-3-oxa-8,10,16-triazadocosan-22-yl)-3,3-dimethyl-5-sulfoindolin-2-ylidene)prop-1-en-1-yl)-3,3-dimethyl-5-sulfo-3*H*-indol-1-ium (2).

To a magnetically stirring solution of CY3.18.OH (25 mg, 34 μmol) in 2 mL of dry DMF in an oven-dried 5 mL round-bottom flask, (*S*)-di-*tert*-butyl 2-(3-((*S*)-6-amino-1-(*tert*-butoxy)-1-oxohexan-2-yl)ureido)pentanedioate, **1** (17 mg, 34 μmol, Astatech, CAS 1025796-31-9, catalog no. W11493), 1-hydroxybenzotriazole (12 mg, 87 μmol), and 7 μL of pyridine were added before condensation was started with EDCI (42 mg, 217 μmol). The reaction was allowed to proceed for 6 h at 27 °C, after which a monosubstituted cy3-amide intermediate was observable by UPLC/MS. At 5 h, 1-azidobutylamine (4 mg, 34 μmol) and additional EDCI (42 mg, 217 μmol of Fluka 03450) were added to the rbf and the reaction was allowed to proceed for 4 more hours at 28 °C. The resulting solution was diluted with DMF (4 mL), and the mixture was loaded onto a preparative HPLC column. Compound **2** was isolated using a H_2O/ACN (0.05% TFA), 50 min elution gradient at a flow rate of 12 mL/min. A linear gradient of increasing ACN from 10% to 70% between 0 and 40 min, followed by a linear increase of ACN from 70% to 90% between 40 and 50 min, was used to elute **2**. Fractions containing **2** were lyophilized in vacuo to yield pure azide **2** as a pink powder. Isolated yield (16 mg, 36%). ^{1}H NMR (500 MHz, DMSO-d_6): δ 8.35 (t, 1H, J = 8.0 Hz), 7.83 (d, 2H, J = 16.5 Hz), 7.77 (t, 1H, J = 5.5 Hz), 7.72 (t, 1H, J = 5.5 Hz), 7.67 (d, 2H, J = 8.5 Hz), 7.38 (d, 2H, J = 8.5 Hz), 6.51 (d, 2H, J = 6.5 Hz), 6.36 (d, 1H, J = 8.5 Hz), 6.31 (d, 1H, J = 7.5 Hz), 4.11 (t, 4H, J = 6.5 Hz), 4.02 (ABq, 1H, J = 8.0, 5.5 Hz), 3.92 (m, 1H), 3.30 (t, 2H, J = 7.0 Hz), 3.02 (ABq, 2H, J = 6.5, 6.0 Hz), 2.98–2.88 (m, 2H), 2.32–2.13 (m, 2H), 2.04 (m, 4H), 1.76–1.66 (m, 16H), 1.60–1.42 (m, 9H), 1.41–1.34 (m, 31H), 1.32–1.14 (m, 5H). ^{13}C NMR (125 MHz, DMSO-d_6):174.2, 172.2, 171.9, 171.7, 171.5, 171.4, 157.1, 149.88, 149.86, 145.8, 145.7, 141.8, 141.7, 140.0, 126.2, 119.8, 110.6, 102.8, 80.5, 80.1, 79.7, 52.9, 52.1, 50.2, 48.93, 48.92, 43.8, 38.0, 37.7, 35.1, 35.0, 31.5, 30.8, 28.7, 27.7, 27.4, 27.3, 26.7, 26.3, 25.75, 25.70, 24.95, 24.92, 22.4. HRMS (ESI)$^-$: *m/z* calculated for [M], $C_{63}H_{95}N_9O_{15}S_2$, 1281.6389; [M – H]$^-$, $[C_{63}H_{94}N_9O_{15}S_2]^-$, 1280.6311; found, 1280.6286 (Δ 1.95 ppm); [M – 2H]$^{2-}$, $[C_{63}H_{93}N_9O_{15}S_2]^{2-}$, 639.8122; found, 639.8108 (δ 2.18 ppm).

((((1-(4-(6-(2-((*E*)-3-((*Z*)-1-(6-(((*S*)-5-Carboxy-5-(3-((*R*)-1,3-dicarboxypropyl)ureido)pentyl)amino)-6-oxohexyl)-3,3-dimethyl-5-sulfoindolin-2-ylidene)prop-1-en-1-yl)-3,3-dimethyl-5-sulfo-3*H*-indol-1-ium-1-yl)hexanamido)butyl)-1*H*-1,2,3-triazol-4-yl)methyl)dimethylammonio)methyl) Trifluoroborate (4).

N-Propargyl-*N*,*N*-dimethylammoniomethyl trifluoroborate ($AMBF_3$) was synthesized according to literature (Liu et al., 2014). Neat trifluoroacetic acid (TFA) (1.0 mL) was added to a stirred solution of **2** (15 mg, 11.7 μmol) at 0 °C. Under continuous stirring, the reaction was warmed to room temperature (25 °C) over a 1 h period. A clean conversion of the *tert*-butyl ester protected acid into a corresponding triacid was observed by UPLC/MS. TFA was removed from the mixture under vacuum. The resulting solid was dissolved in a solution of 1.0 M $CuSO_4$ (200 μL) and ascorbic acid (1.0 M, 400 μL). $AMBF_3$ (2.9 mg, 17.5 μmol) in DMF (1.5 mL) was added to the solution. Huisgen 1,3-dipolar cycloaddition proceeded at room temperature for 3 h. The resulting mixture was filtered through Celite and washed with

DMF (2 mL). The filtrate was directly loaded onto a preparative HPLC, and **4** was isolated using a H_2O/ACN (0.05% TFA) 50 min elution gradient at a flow rate of 12 mL/min. A linear gradient of increasing ACN from 10% to 60% between 0 and 40 min, followed by a linear increase of ACN from 60% to 90% between 40 and 50 min, was used to elute **4**. The fractions containing the desired product were lyophilized in vacuo to yield chemically pure **4** as a pink powder. Isolated yield (8.0 mg, 53%). ^{1}H NMR (500 MHz, DMSO-d6): δ 8.80 (s, 0.35H), 8.38–8.32 (m, 2H), 7.82–7.65 (m, 6H), 7.40–7.37 (m, 2H), 6.51 (d, 2H, J = 13.5 Hz), 6.35 (dd, J = 8.0, 21.0 Hz), 4.90 (s, 0.5 H), 4.66–4.59 (m, 1H), 4.54–4.49 (m, 2H), 4.39 (t, 2H, J = 7.0 Hz), 4.20–3.94 (m, 16H), 3.20–3.06 (m, 2H), 3.01–2.90 (m, 8H), 2.29–2.21 (m, 3H), 2.08–1.97 (m, 4H), 1.97–1.85 (m, 1H), 1.69 (s, 12H), 1.61–1.44 (m, 6H), 1.40–1.27 (m, 8H), 1.27–1.17 (m, 3H). ^{19}F NMR (470 MHz, DMSO-d_6): δ 137.32. HRMS (ESI): *m/z* calculated for [M], $C_{57}H_{82}BF_3N_{10}O_{15}S_2$, 1278.5448; [M + 2[-F]], calcd 630.2770, found 630.2765 (Δ 0.81 ppm).

The optical properties of [^{19}F]-**4** are similar to Cy3.18.OH (pH 7.5, 1× PBS, (Supporting Information Table 1)). At physiological pH (1× PBS, 1 mM PBS, pH 7.5), [^{19}F]-**4** has an extinction coefficient of 159 000 M^{-1} cm^{-1} (Figure 1B, ε_{max} = 540 nm) and an excitation maximum λ= 563 nm, with Stokes shift of 13 nm). [^{19}F]-**4** has a quantum yield of φ = 0.06 (6%), 150% that of Cy3.18.OH.

Radiochemistry.

The radiolabeling of [^{19}F]-**4** is performed in 25 min. In a typical synthesis, 13.5 mCi of [^{18}F]-**4** (at a molar activity of 192 mCi/μmol) was isolated starting with 56.2 mCi of [^{18}F]-fluoride ion (Figure 1C). Isotope exchange[21] proceeds in one step under aqueous, acidic pH conditions (pH = 2.0, pyridazine–HCl buffer, 10 μL) and proceeds quickly (10–15 min) at high temperatures (80–90 °C). Removal of unreacted [^{18}F]-fluoride ion is performed by passing the [^{18}F]-**4** reaction mixture through a prewashed (5 mL, deionized water) C18 cartridge (Waters no. 186005125). A 20–23 mL volume of water is used to flush contaminating [^{18}F]-fluoride ion from the cartridge. [^{18}F]-**4**, bound to the cartridge, is eluted with a 4.0 mM HCl in ethanol (99%). All steps involving the cartridge were performed using a syringe pump set to deliver at a 40 mL/h flow rate. A slow mobile-phase flow rate is key, as impatience in [^{18}F]-**4** purification will result in the elution of [^{18}F]-**4** that is contaminated with [^{18}F]-fluoride ion.[21] Resulting [^{18}F]-**4** in acidic ethanol is immediately diluted 10-fold with 1 mM phosphate buffered saline (1× PBS) and filtered through a 0.22 μm filter. The resulting pH 7.4 filtrate is injected intravenously. As observed in Liu et al. in related radiochemistry,[21] a minor quantity (<5%) of borate (defluoridated) trifluoroborate is observed during acidic isotopic exchange reaction or lyophilization. This product does not emit a positron, is not visible by PET, and can be reconverted into the trifluoroborate by treatment with acidic fluoride. Liberation of [^{18}F]-fluoride ion from [^{19}F]-**4** (defluoridation) is not observed in vivo (Figure 4A).

Quantification of EC_{50} by γ-Scintillation.

Suspensions of 2.5 × 10^5 PC3 or PC3-PIP cells are incubated with 1.25–160 nM solutions of nonradiolabeled [^{19}F]-**4**, where each aliquot also contains 1 μCi of [^{18}F]-**4**. After 1 h incubation at room temperature, cells are washed, then pelleted by centrifuge. Activity in

isolated pellets and supernatants is analyzed using a Wallac Wizard 3.0 γ-counter. EC_{50} is determined by plotting radioactive pellet fractions in exponential rise-to-max functions using SigmaPlot 11.0 ($f = a \exp(-bx)$) (Figure 1D).

In Vivo Imaging and Biodistribution Analysis.

Procedures in C57BL/6 male mice (5- to 6-week-old, 20–25 g, Charles River Laboratories) are conducted in studies that are approved by the Weill Cornell Medical Center Institutional Animal Care and Use Committee (no. 2014-0030) and are consistent with the recommendations of the American Veterinary Medical Association and the National Institutes of Health Guide for the Care and Use of Laboratory Animals. Suspensions of 3×10^6 (18 mg) PC3 and PC3-PIP cells are weighed and injected subcutaneously into the left and right flank of mice ($n = 6$) respectively. Mice ($n = 5$) not bearing cell injections are set as controls. A 100 μL volume of [^{18}F]-**4** (80 μCi, 25 μM) is injected into mice through the lateral tail vein. A 10 min CT scan followed by a 15 min PET is acquired at 2 and 6 h after injection. CT/PET images are processed with Amide version 1.0.4 open source software.

Mice are sacrificed by cervical dislocation 2 h after injection. [^{18}F]-**4** content in harvested brain, heart, lung, stomach, liver, kidneys, intestine, spleen and the myocutaneous tissue bearing PC3 and PC3-PIP injections are quantified by γ-scintillation using a Wallac Wizard 3.0 γ-counter. [^{18}F]-**4** in vivo and ex vivo fluorescent imaging are performed 24–48 h after injection, at a time point where ^{18}F has decayed quantitatively and animals or tissues are no longer radioactive. This delay mimics clinical delay that would occur between nuclear medicine analysis and PCa surgery. Fluorescent analysis is performed on a Bruker In-Vivo Xtreme imaging system with an exposure time of 20 s. Excitation and emission wavelengths are set as 550 and 600 nm, respectively. PET/CT images are generated using Bruker molecular imaging software.

Supplementary Material

Refer to Web version on PubMed Central for supplementary material.

ACKNOWLEDGMENTS

The project was supported by National Institutes of Health Grants EB013904, R01CA178007, and P30CA008748.

ABBREVIATIONS USED

PSMA	prostate specific membrane
AMBF$_3$	ammonium trifluoroborate
PCa	prostate cancer
PET	positron emission tomography
FL	fluorescence
CT	computed tomography

DIPEA	*N,N*-diisopropylethylamine
EDCI	1-ethyl-3-(3-(dimethylaminopropyl)carbodiimide

REFERENCES

(1). Stangelberger A; Waldert M; Djavan B Prostate cancer in elderly men. Rev. Urol 2008, 10, 111–119. [PubMed: 18660852]

(2). Jemal A; Siegel R; Ward E; Hao Y; Xu J; Thun MJ Cancer statistics, 2009. Ca-Cancer J. Clin 2009, 59, 225–249. [PubMed: 19474385]

(3). National Hospital Discharge Survey. CDC/NCHS, 2010.

(4). Hall MA; Pinkston KL; Wilganowski N; Robinson H; Ghosh P; Azhdarinia A; Vazquez-Arreguin K; Kolonin AM; Harvey BR; Sevick-Muraca EM Comparison of mAbs targeting epithelial cell adhesion molecule for the detection of prostate cancer lymph node metastases with multimodal contrast agents: quantitative small-animal PET/CT and NIRF. J. Nucl. Med 2012, 53, 1427–1437. [PubMed: 22872743]

(5). Auffenberg GB; Linsell S; Dhir A; Myers SN; Rosenberg B; Miller DC Comparison of pathological outcomes for men with low risk prostate cancer from diverse practice settings: Similar results from immediate prostatectomy or initial surveillance with delayed prostatectomy. J. Urol 2016, 196, 1415–1421. [PubMed: 27256204]

(6). Sfoungaristos S; Perimenis P Bilateral cancer in prostate biopsy associates with the presence of extracapsular disease and positive surgical margins in low risk patients: a consideration for bilateral nerve sparing radical prostatectomy decision. Urol. J 2013, 10, 966–972. [PubMed: 24078504]

(7). Foss CA; Mease RC; Fan H; Wang YC; Ravert HT; Dannals RF; Olszewski RT; Heston WD; Kozikowski AP; Pomper MG Radiolabeled small-molecule ligands for prostate-specific membrane antigen: In vivo imaging in experimental models of prostate cancer. Clin. Cancer Res 2005, 11, 4022–4028. [PubMed: 15930336]

(8). Benesova M; Schafer M; Bauder-Wust U; Afshar-Oromieh A; Kratochwil C; Mier W; Haberkorn U; Kopka K; Eder M Preclinical evaluation of a tailor-made DOTA-conjugated PSMA inhibitor with optimized linker moiety for imaging and endoradiotherapy of prostate cancer. J. Nucl. Med 2015, 56, 914–920. [PubMed: 25883127]

(9). Weineisen M; Simecek J; Schottelius M; Schwaiger M; Wester HJ Synthesis and preclinical evaluation of DOTAGA-conjugated PSMA ligands for functional imaging and endoradiotherapy of prostate cancer. EJNMMI Res 2014, 4, 63. [PubMed: 26116124]

(10). Eder M; Schafer M; Bauder-Wust U; Hull WE; Wangler C; Mier W; Haberkorn U; Eisenhut M 68Ga-complex lipophilicity and the targeting property of a urea-based PSMA inhibitor for PET imaging. Bioconjugate Chem 2012, 23, 688–697.

(11). Bailey J; Wuest M; Bouvet V; Bergman C; Janzen N; Genady A; Valliant JF; Schirrmacher R; Wuest F Silicon/Fluorine-18/PSMA: A winning team for PET imaging of prostate Cancer. J. Labelled Compd. Radiopharm 2017, 60 (Suppl. 1), S353.

(12). Tsien RY Imagining imaging's future. Nat. Rev. Mol. Cell Biol 2003, No. Suppl., SS16–SS21. [PubMed: 14587522]

(13). Humblet V; Lapidus R; Williams LR; Tsukamoto T; Rojas C; Majer P; Hin B; Ohnishi S; De Grand AM; Zaheer A; Renze JT; Nakayama A; Slusher BS; Frangioni JV High-affinity near-infrared fluorescent small-molecule contrast agents for in vivo imaging of prostate-specific membrane antigen. Mol. Imaging 2005, 4, 448–462. [PubMed: 16285907]

(14). Nakajima T; Mitsunaga M; Bander NH; Heston WD; Choyke PL; Kobayashi H Targeted, activatable, in vivo fluorescence imaging of prostate-specific membrane antigen (PSMA) positive tumors using the quenched humanized J591 antibody-indocyanine green (ICG) Conjugate. Bioconjugate Chem 2011, 22, 1700–1705.

(15). Sonn GA; Behesnilian AS; Jiang ZK; Zettlitz KA; Lepin EJ; Bentolila LA; Knowles SM; Lawrence D; Wu AM; Reiter RE Fluorescent image-guided surgery with an anti-prostate stem

cell antigen (PSCA) diabody enables targeted resection of mouse prostate cancer xenografts in real time. Clin. Cancer Res 2016, 22, 1403–1412. [PubMed: 26490315]

(16). Lutje S; Rijpkema M; Franssen GM; Fracasso G; Helfrich W; Eek A; Oyen WJ; Colombatti M; Boerman OC Dualmodality image-guided surgery of prostate cancer with a radiolabeled fluorescent anti-PSMA monoclonal antibody. J. Nucl. Med 2014, 55, 995–1001. [PubMed: 24700882]

(17). Baranski AC; Schafer M; Bauder-Wust U; Roscher M; Schmidt J; Stenau E; Simpfendorfer T; Teber D; Maier-Hein L; Hadaschik B; Haberkorn U; Eder M; Kopka K PSMA-11 Derived dual-labeled PSMA-inhibitors for preoperative PET imaging and precise fluorescence-guided surgery of prostate cancer. J. Nucl. Med 2018, 59, 639–645. [PubMed: 29191856]

(18). Schirrmacher R; Bradtmoller G; Schirrmacher E; Thews O; Tillmanns J; Siessmeier T; Buchholz HG; Bartenstein P; Wangler B; Niemeyer CM; Jurkschat K ^{18}F-labeling of peptides by means of an organosilicon-based fluoride acceptor. Angew. Chem., Int. Ed 2006, 45, 6047–6050.

(19). Liu ZB; Pourghiasian M; Radtke MA; Lau J; Pan JH; Dias GM; Yapp D; Lin KS; Benard F; Perrin DM An organotrifluoroborate for broadly applicable one-step F-18-labeling. Angew. Chem., Int. Ed 2014, 53, 11876–11880.

(20). Liu ZB; Li Y; Lozada J; Wong MQ; Greene J; Lin KS; Yapp D; Perrin DM Kit-like F-18-labeling of RGD-F-19-Arytrifluroborate in high yield and at extraordinarily high specific activity with preliminary in vivo tumor imaging. Nucl. Med. Biol 2013, 40, 841–849. [PubMed: 23810487]

(21). Liu Z; Lin KS; Benard F; Pourghiasian M; Kiesewetter DO; Perrin DM; Chen X One-step ^{18}F labeling of biomolecules using organotrifluoroborates. Nat. Protoc 2015, 10, 1423–1432. [PubMed: 26313478]

(22). Afshar-Oromieh A; Zechmann CM; Malcher A; Eder M; Eisenhut M; Linhart HG; Holland-Letz T; Hadaschik BA; Giesel FL; Debus J; Haberkorn U Comparison of PET imaging with a ^{68}Ga-labelled PSMA ligand and ^{18}F-choline-based PET/CT for the diagnosis of recurrent prostate cancer. Eur. J. Nucl. Med. Mol. Imaging 2014, 41, 11–20. [PubMed: 24072344]

(23). Tiffany CW; Lapidus RG; Merion A; Calvin DC; Slusher BS Characterization of the enzymatic activity of PSM: comparison with brain NAALADase. Prostate 1999, 39, 28–35. [PubMed: 10221263]

(24). Bernard-Gauthier V; Bailey JJ; Liu ZB; Wangler B; Wangler C; Jurkschat K; Perrin DM; Schirrmacher R From unorthodox to established: The current status of ^{18}F-trifluoroborate- and ^{18}F-SiFA-based radiopharmaceuticals in PET nuclear imaging. Bioconjugate Chem 2016, 27, 267–279.

(25). An FF; Chan M; Kommidi H; Ting R Dual PET and near-infrared fluorescence imaging probes as tools for imaging in oncology. AJR, Am. J. Roentgenol 2016, 207, 266–273. [PubMed: 27223168]

(26). Bouchelouche K; Choyke PL; Capala J Prostate specific membrane antigen- a target for imaging and therapy with radionuclides. Discovery Med 2010, 9, 55–61.

(27). Weineisen M; Schottelius M; Simecek J; Baum RP; Yildiz A; Beykan S; Kulkarni HR; Lassmann M; Klette I; Eiber M; Schwaiger M; Wester HJ 68Ga- and 177Lu-labeled PSMA I&T: Optimization of a PSMA-targeted theranostic concept and first proof-of-concept human studies. J. Nucl. Med 2015, 56, 1169–1176. [PubMed: 26089548]

(28). Szabo Z; Mena E; Rowe SP; Plyku D; Nidal R; Eisenberger MA; Antonarakis ES; Fan H; Dannals RF; Chen Y; Mease RC; Vranesic M; Bhatnagar A; Sgouros G; Cho SY; Pomper MG Initial evaluation of [^{18}F]DCFPyL for prostate-specific membrane antigen (PSMA)-targeted PET imaging of prostate cancer. Mol. Imaging Biol 2015, 17, 565–574. [PubMed: 25896814]

(29). Chen Y; Dhara S; Banerjee SR; Byun Y; Pullambhatla M; Mease RC; Pomper MG A low molecular weight PSMA-based fluorescent imaging agent for cancer. Biochem. Biophys. Res. Commun 2009, 390, 624–629. [PubMed: 19818734]

(30). Afshar-Oromieh A; Haberkorn U; Eder M; Eisenhut M; Zechmann CM [^{68}Ga]Gallium-labelled PSMA ligand as superior PET tracer for the diagnosis of prostate cancer: comparison with 18F-FECH. Eur. J. Nucl. Med. Mol. Imaging 2012, 39, 1085–1086. [PubMed: 22310854]

(31). Hillier SM; Maresca KP; Lu G; Merkin RD; Marquis JC; Zimmerman CN; Eckelman WC; Joyal JL; Babich JW 99mTc-labeled small-molecule inhibitors of prostate-specific membrane antigen

for molecular imaging of prostate cancer. J. Nucl. Med 2013, 54, 1369–1376. [PubMed: 23733925]

(32). Chen Y; Pullambhatla M; Foss CA; Byun Y; Nimmagadda S; Senthamizhchelvan S; Sgouros G; Mease RC; Pomper MG 2-(3-{1-Carboxy-5-[(6-[^{18}F]fluoro-pyridine-3-carbonyl)-amino]-pentyl}-ureido)-pen tanedioic acid, [18F]DCFPyL, a PSMA-based PET imaging agent for prostate cancer. Clin. Cancer Res 2011, 17, 7645–7653. [PubMed: 22042970]

(33). Evans JD; Jethwa KR; Ost P; Williams S; Kwon ED; Lowe VJ; Davis BJ Prostate cancer-specific PET radiotracers: A review on the clinical utility in recurrent disease. Pract Radiat Oncol 2018, 8, 28–39. [PubMed: 29037965]

(34). Mujumdar RB; Ernst LA; Mujumdar SR; Lewis CJ; Waggoner AS Cyanine dye labeling reagents: sulfoindocyanine succinimidyl esters. Bioconjugate Chem 1993, 4, 105–111.

(35). Liu Z; Chao D; Li Y; Ting R; Oh J; Perrin DM From minutes to years: Predicting organotrifluoroborate solvolysis rates. Chem. - Eur. J 2015, 21, 3924–3928. [PubMed: 25639468]

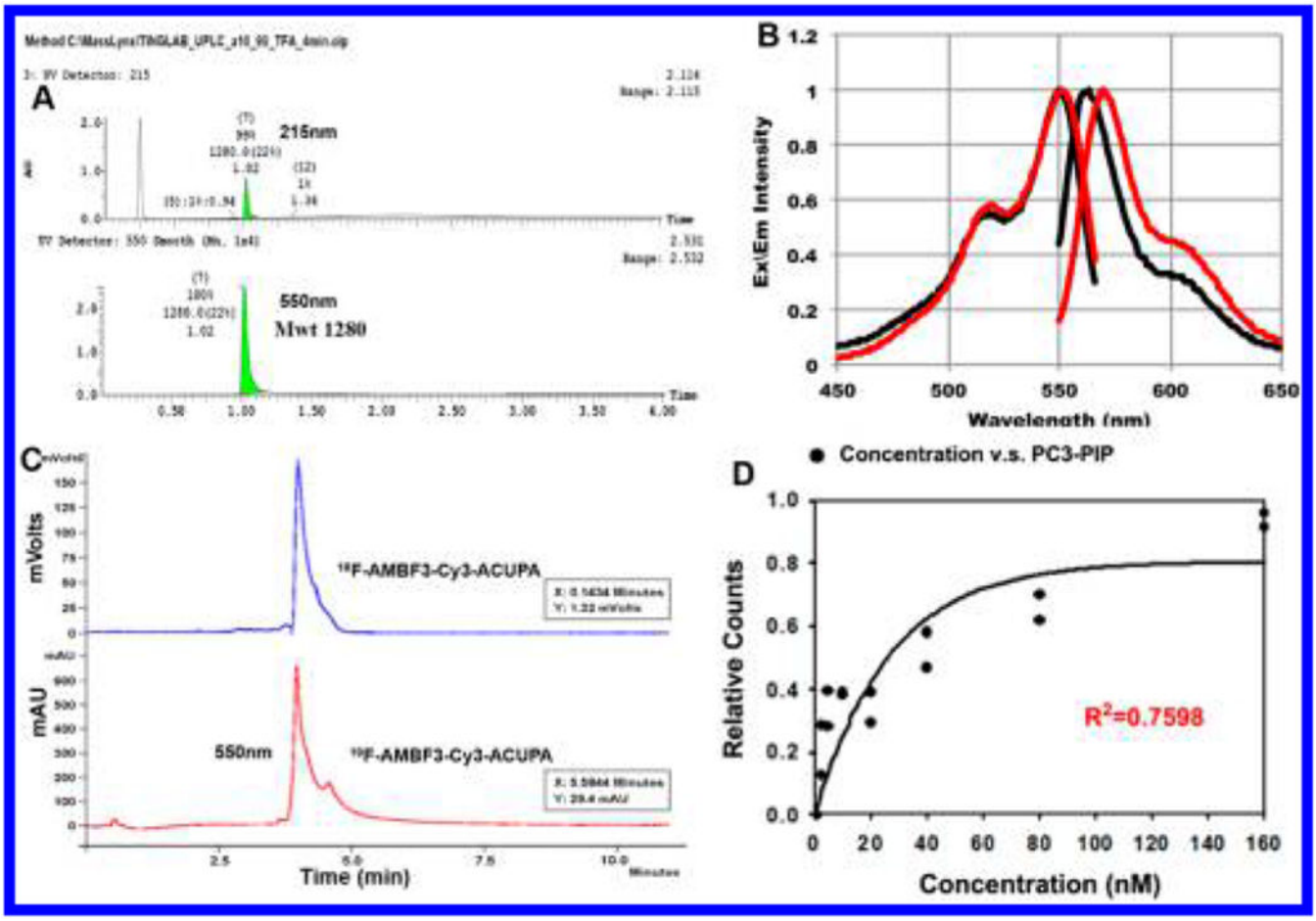

Figure 1.

Spectral and radiochemical properties of [$^{18/19}$F]-**4**. (A) Ultraperformance liquid chromatography (UPLC) absorbance (215 and 550 nm) elution profile of purified [^{19}F]-**4**. (B) Excitation and emission spectra of 2–4 μM solutions of Cy3 (black) and [^{19}F]-**4** (red) in 1× PBS, pH 7.4, measured on a Cary Eclipse spectrophotometer with 5 nm slit widths and excitation at 540 nm. (C) Reverse-phase HPLC of radiolabeled [^{18}F]-**4**. A single radioactive peak is observed. (D) Scintillation analysis demonstrates PSMA-specific [^{18}F]-**4** binding to PC3-PIP cells (see Supporting Information for PC3 control).

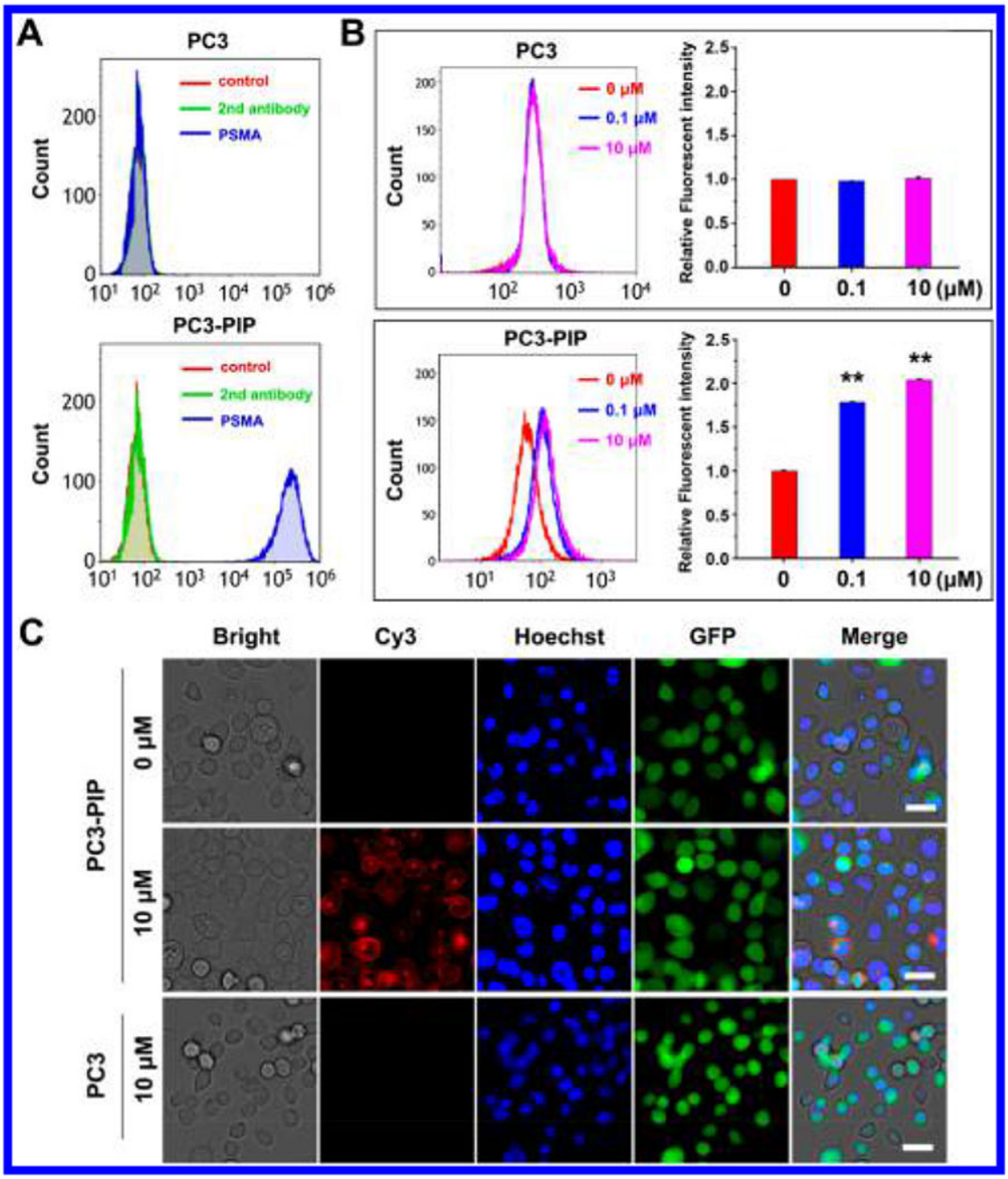

Figure 2.

Authentication of cell lines and demonstration of [^{19}F]-**4** affinity to PSMA-negative PC3 and PSMA positive PC3-PIP cells by flow cytometry and epifluorescent microscopy. (A) PSMA expression on PC3 and PC3-PIP luciferase and GFP expressing cells is confirmed by flow cytometry (primary J591 antibody followed by APC secondary antibody staining is used to verify PSMA expression). (B) FACS flow cytometry is used to measure [^{19}F]-**4** affinity to cells at 0.1 and 10 μM (incubation was performed for 1 h at 37 °C). Data are acquired with 488 nm, 22 mW laser excitation and a 620/30 emission filter. (C) Epifluorescent microscopy

is used to confirm FACS data in (B). From left to right, [^{19}F]-**4** and Hoechst 33342 (0.1 μg/mL) stained PC3 and PC3-PIP cells are analyzed by bright field Cy3 fluorescence (PSMA, red, ex/em = 531/593 nm), Hoechst fluorescence (nuclear stain, blue, ex/em = 357/447 nm), and green fluorescent protein (GFP) fluorescence (lentivirally transduced GFP expression, green, ex/em = 470/510 nm). [^{19}F]-**4** membrane localization to only PC3-PIP cells (red) is observed. Fluorescence is visible on PC3-PIP cells only. Data are presented as the mean ± SD. Scale bar = 25 μm.

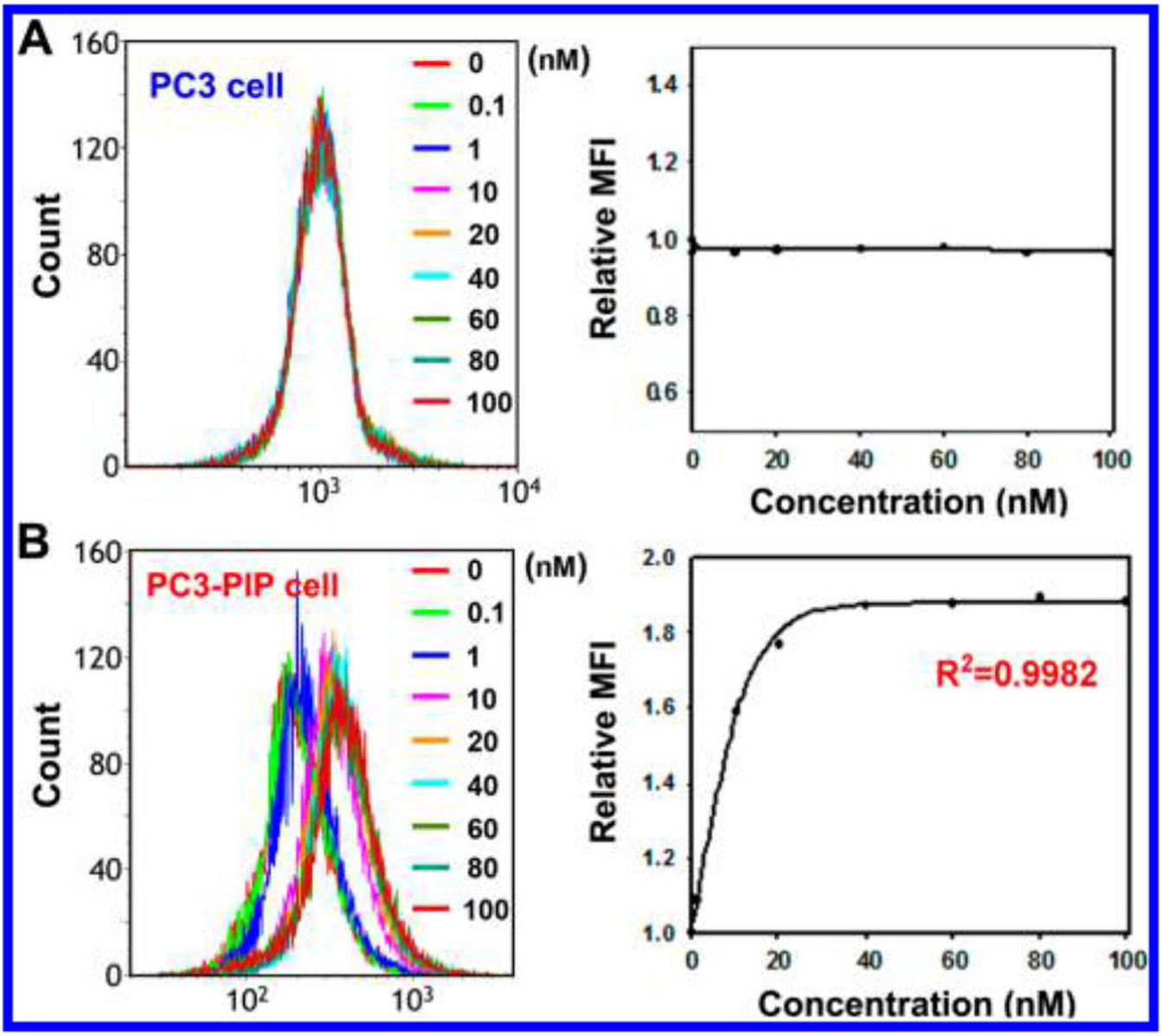

Figure 3.

In vitro fluorescent confirmation of nanomolar [^{19}F]-**4**-PSMA specificity. Binding efficacy (EC_{50}) measurements between [^{19}F]-**4** and PC3 (A, PSMA−) and PC3-PIP (B, PSMA+) cells as determined by FACS in the Cy3 channel (data are acquired with 488 nm, 22 mW laser excitation and a 620/30 emission filter). [^{19}F]-**4**-PC3-PIP EC_{50} is 6.74 ± 1.33 nM. Cells are incubated with 0.1–100 nM [^{19}F]-**4** for 1 h at 37 °C. EC_{50} is calculated by Sigma Plot 10.0 software using nonlinear approximations in single, two-parameter exponential decay functions ($f = a\exp(-bx)$). MFI = mean fluorescent intensity.

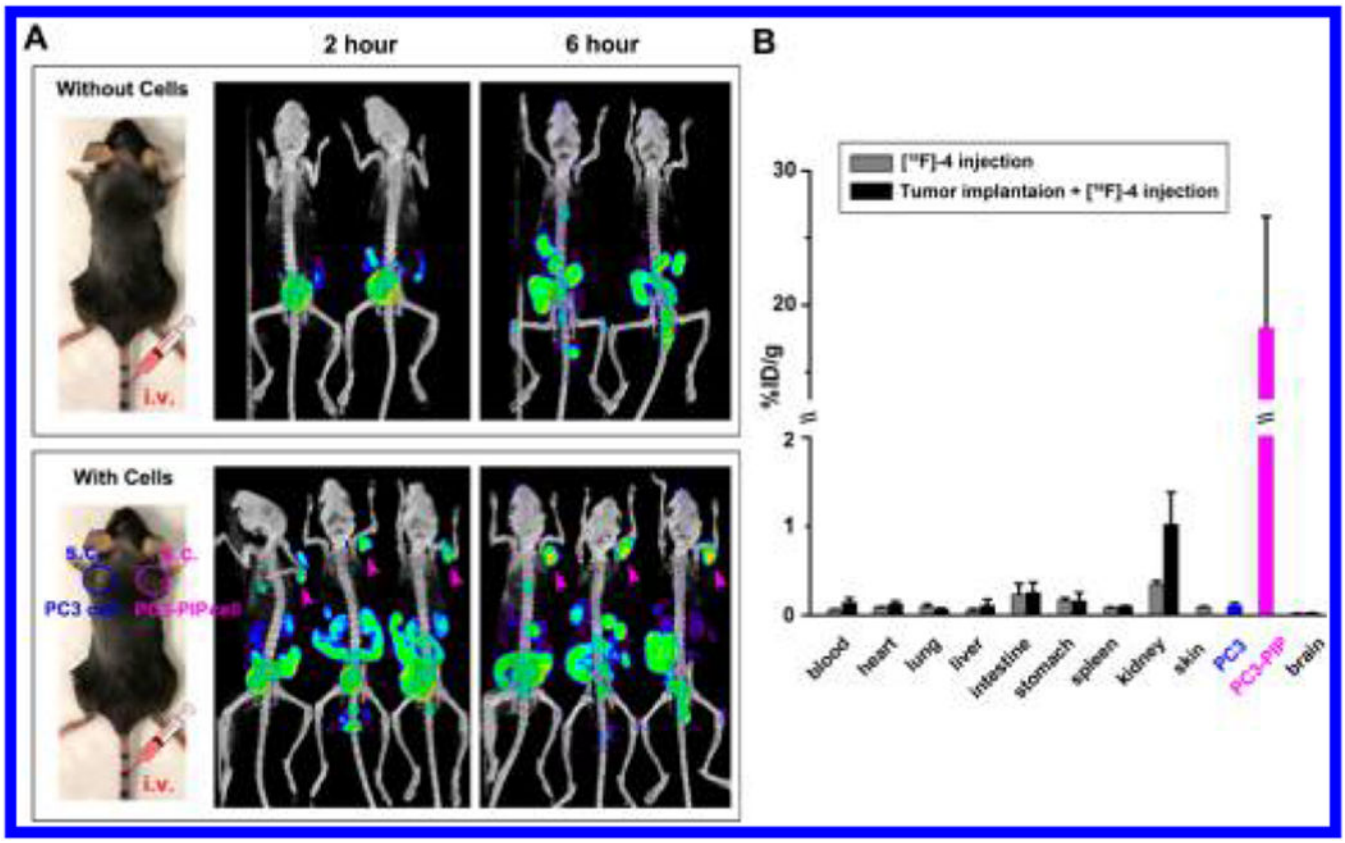

Figure 4.

In vivo PET/CT confirmation of [^{18}F]-**4**-PSMA specificity. (A) PET (NIH color table)/CT (white) assessment of [^{18}F]-**4** binding to PSMA+ cell containing myocutaneous tissue (bottom panel, right flank of three mice, pink arrow). (A, Bottom panel) Mice are inoculated subcutaneously in opposite flanks with 3 million PC3 cells (PSMA−, left flank) and PC3-PIP cells (PSMA+, right flank). Mice without cell inoculation serve as controls (A, top panel). Mice are intravenously injected with 80 μCi of [^{18}F]-**4**, 15 min following inoculation. At 2 and 6 h after [^{18}F]-**4** injection, mice are imaged using a 10 min CT followed by a 15 min PET scanning protocol. All PET/CT data are shown as maximum intensity projections (MIP). (B) μ-Scintillated biodistribution of [^{18}F]-**4** in mice 2 h after injection. Main organs are collected, weighed, and scintillated on a Wallac Wizard 3.0 μ-counter. Data are presented as mean ± SEM.

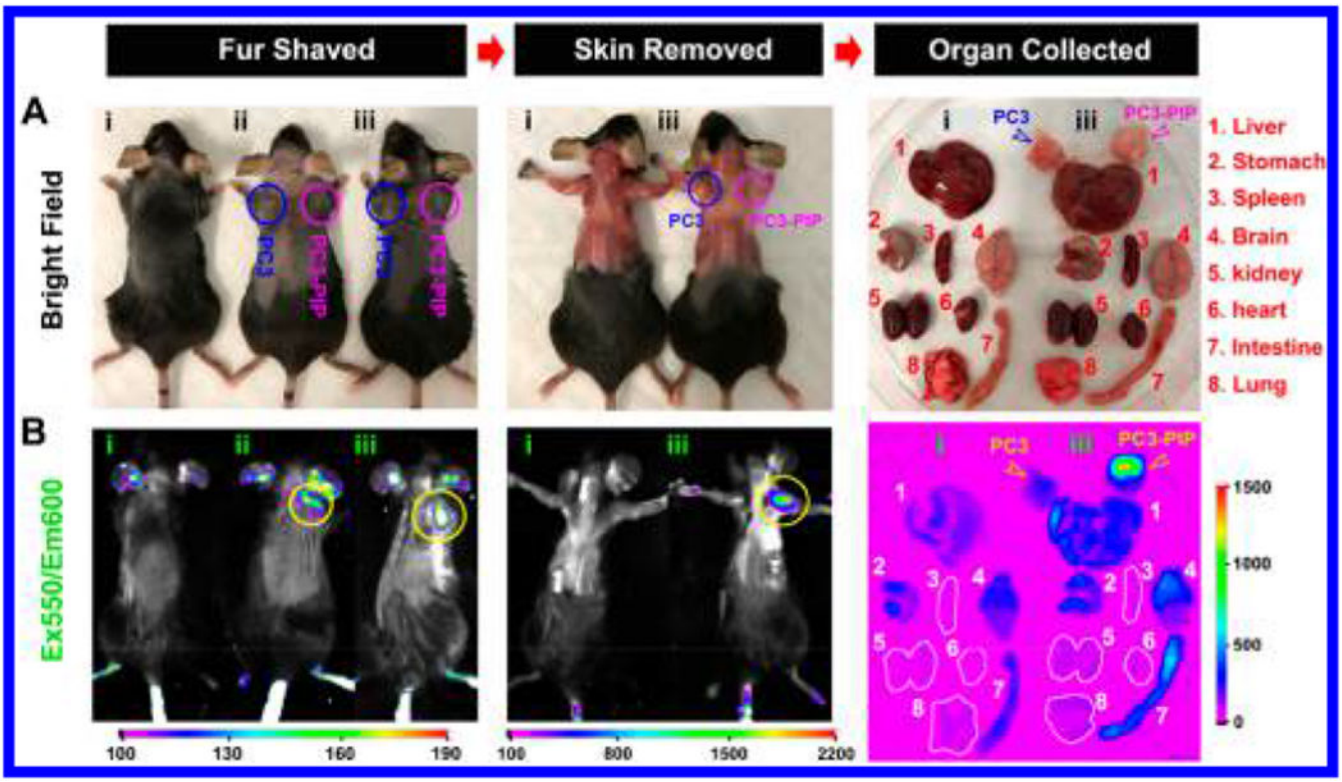

Figure 5.

In vivo/ex vivo fluorescence confirmation of [^{19}F]-**4**-PSMA specificity. Mice are inoculated subcutaneously in opposite flanks with (i) no cells and 3 million PC3 cells (ii and iii, PSMA −, left flank, blue circle) and PC3-PIP cells (ii and iii, PSMA+, right flank, magenta circle). All mice receive [^{18}F]-**4** (25 μM, 100 μL) intravenously through the tail vein, 15 min after inoculation. After 24 h, mice are shaved, sacrificed, and skin is removed in preparation for fluorescent full-field imaging. Following imaging, organs are harvested and placed on a Petri dish for fluorescent and bright field analyses (right column). In all steps, mice and tissues are observed by fluorescence imaging. (A) Dorsal, bright field images of mice and harvested organs. (B) PSMA specific fluorescent [^{19}F]-**4** (550/600 nm ex/em) binding in PC3-PIP bearing tissue is indicated with yellow arrows/circles. [^{19}F]-**4** binding to PC3 (Control) cells is not observed. Exposure time is 20 s in a Bruker extreme fluorescence monitoring device. Relative mean fluorescence intensity is estimated in different tissues (Supporting Information Figure S2).

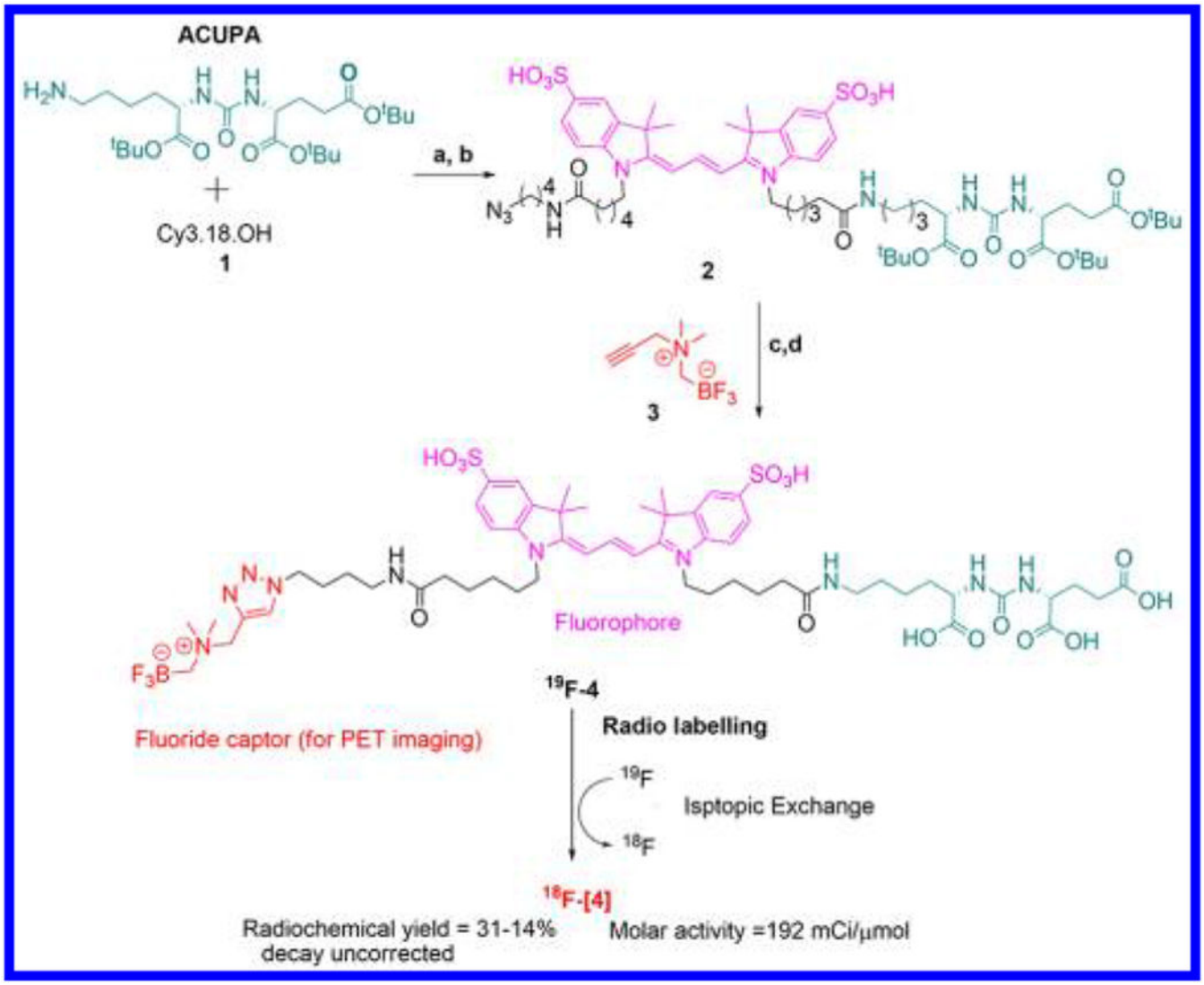

Scheme 1. Synthesis of [$^{18/19}$F]-4, a PET/FL PSMA Inhibitor[a]

[a]Synthesis: (a) 1.0 equiv of CY3.18.OH, 1.0 equiv of ACUPA, 2.5 equiv of HOBt, 2.5 equiv of pyridine, 4.0 equiv of EDCI, DMF, rt, N_2, 6 h; (b) 1.2 equiv of 1-azidobutylamine, rt, 2 h; (c) 0.5 mL of TFA, 1 h; (d) 1.0 equiv of 1 M $CuSO_4 \cdot 5H_2O$, 2.0 equiv of 1 M ascorbic acid, DMF, rt, 3 h. Radiolabeling: 1 M pyridazine–HCl, pH = 2.5, ≤50 mCi aqueous [^{18}F]-fluoride ion (Specific concentration of >1.5 Ci/mL), 80–90 °C.